Melanoma tumour vasculature heterogeneity: from mice models to human

Vincent Pautu, Adélie Mellinger, Pauline Resnier, Elise Lepeltier, Ludovic Martin, Lise Boussemart, Franck Letournel, et al.

Journal of Cancer Research and Clinical Oncology

ISSN 0171-5216

J Cancer Res Clin Oncol
DOI 10.1007/s00432-018-2809-z

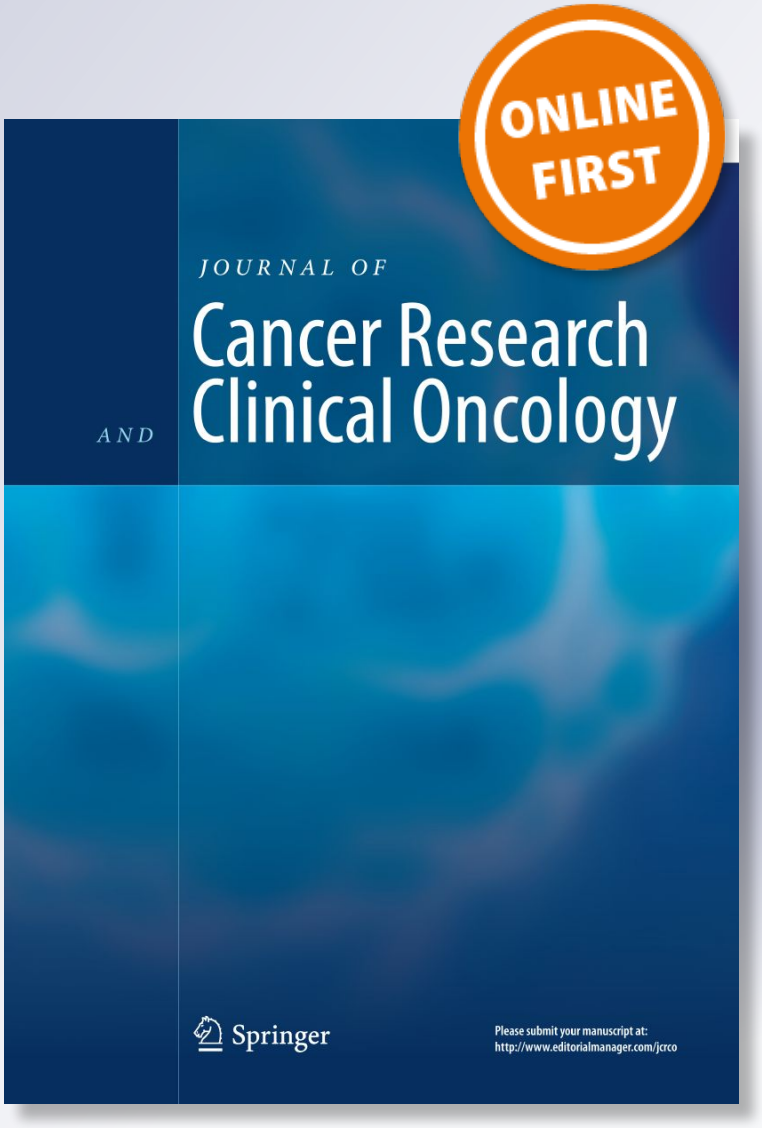

Springer

Journal of Cancer Research and Clinical Oncology
https://doi.org/10.1007/s00432-018-2809-z

ORIGINAL ARTICLE – CANCER RESEARCH

Melanoma tumour vasculature heterogeneity: from mice models to human

Vincent Pautu[1] · Adélie Mellinger[1] · Pauline Resnier[1] · Elise Lepeltier[1] · Ludovic Martin[2] · Lise Boussemart[3,4] · Franck Letournel[1] · Catherine Passirani[1] · Nicolas Clere[1]

Received: 5 September 2018 / Accepted: 30 November 2018

Abstract

Tumour angiogenesis is defined by an anarchic vasculature and irregularities in alignment of endothelial cells. These structural abnormalities could explain the variability in distribution of nanomedicines in various tumour models. Then, the main goal of this study was to compare and to characterize the tumour vascular structure in different mouse models of melanoma tumours (B16F10 and SK-Mel-28) and in human melanomas from different patients. Tumours were obtained by subcutaneous injection of 10^6 B16F10 and 3.10^6 SK-Mel-28 melanoma cells in C57BL/6 and nude mice, respectively. Tumour growth was evaluated weekly, while vasculature was analysed through fluorescent labelling via CD31 and desmin. Significant differences in tumour growth and mice survival were evidenced between the two melanoma models. A fast evolution of tumours was observed for B16F10 melanoma, reaching a tumour size of 100 mm^3 in 7 days compared to SK-Mel-28 which needed 21 days to reach the same volumes. Important differences in vascularization were exposed between the melanoma models, characterized by a significant enhancement of vascular density and a significant lumen size for mice melanoma models compared to human. Immunostaining revealed irregularities in endothelium structure for both melanoma models, but structural differences of vasculature were observed, characterized by a stronger expression of desmin in SK-Mel-28 tumours. While human melanoma mainly develops capillaries, structural irregularities are also observed on the samples of this tumour model. Our study revealed an impact of cell type and tumour progression on the structural vasculature of melanoma, which could impact the distribution of drugs in the tumour environment.

Keywords Melanoma · Tumour vasculature heterogeneity · Endothelium · Microcirculation

Introduction

Angiogenesis, a critical step in tumorigenesis, is defined as cellular processes leading to the formation of new blood vessels from pre-existing vasculature (Carmeliet and Jain 2000). Many solid tumours are known to stimulate angiogenesis to create vasculature required for their growth, spread, and metastasis (Hanahan and Weinberg 2000, 2011).

As for all solid tumours, melanoma growth needs a high angiogenic activity, an important step in melanoma metastasis (Elder et al. 1996; Tuthill and Reed 2007). Vascularization is characterized by a monolayer of endothelial cells surrounded by one or more layers of smooth muscle cells and supporting cells such as pericytes, whose localization is on the basal lamina of the vascular endothelium. Angiogenesis is characterized by an angiogenic switch, i.e., an imbalance between pro-angiogenic factors, such as VEGF, fibroblast growth factors (FGF-1, FGF-2), platelet-derived growth factor (PDGF-B and PDGF-C), and anti-angiogenic factor production, such as thrombospondin-1 (TSP-1) (Folkman 2002). Furthermore, tumour vasculature is characterized by tortuous ramifications, heterogeneity in their diameter, distribution and density (Baluk et al. 2005). This anarchic vasculature gives rise to heterogeneous blood flow,

✉ Nicolas Clere
nicolas.clere@univ-angers.fr

[1] UMR Inserm 1066, CNRS 6021, Université d'Angers, CHU, IBS, IRIS, MINT, UNIV Angers, INSERM, CNRS, Université Bretagne Loire, IBS-CHU, 4, rue Larrey, 49933 Angers, France

[2] CHU Angers, 4 rue Larrey, 49933 Angers, France

[3] Department of Dermatology, Pontchaillou Hospital, CHU de Rennes, 35000 Rennes, France

[4] Univ Rennes, CNRS, IGDR, UMR 6290, 35000 Rennes, France

Published online: 13 December 2018

defined by poor perfusion of plasma and hypoxic regions in tumours (Jain and Baxter 1988). Thereby, in tumour vessels, it has been reported some irregularities in alignment of endothelial cells and a lack of pericyte cells (Armulik et al. 2011). Furthermore, perivascular smooth muscle is often lacking in tumour vessels, making them poorly reactive to normal vasoregulation (Chan et al. 1984). These changes enhance vascular permeability through an increase in gap formation between endothelial cells (0.1–3 µm in diameter) that promotes release of macromolecules into extravascular compartment (Danquah et al. 2011; McDonald et al. 1999; Matsumura and Maeda 1986).

Improved efficacy of treatments through modulation of tumour endothelium has been largely described in melanoma mice models (Bolkestein et al. 2016; Duncan et al. 2013). However, despite numerous preclinical studies, only few studies attempt to show the interest of the modification of tumour endothelium in clinical trial (Stirland et al. 2013): no study has been focused on the evaluation of the vascular structure in human tumours, compared to mice models. Therefore, this study aims to analyse the vascular structure of different melanomas from human and mice models to determine differences and correlations between them.

Materials and methods

SK-Mel-28 and B16F10 melanoma cell culture

The SK-Mel-28 human melanoma cell line, obtained from ATCC (LGC Promochem, Molsheim, France), and B16F10 mouse melanoma cell line (gift from University of Brussels) were grown in RPMI-1640 medium (Lonza, Verviers, Belgium) supplemented with 10% foetal bovine serum (Lonza, Verviers, Belgium), 10 units of penicillin, 10 mg of streptomycin, 25 µg/mL of amphotericin B (Sigma-Aldrich, Saint Louis, USA), and 1% non-essential amino acids (Lonza). Cell lines were cultured according to ATCC protocol and maintained at 37 °C in a humidified atmosphere with 5% CO_2.

In vivo tumour development

Ethical approval

All procedures involving animals, including the breeding protocols, were conducted in accordance with protocols approved by the ethical committee of the University of Angers and the regional ethics committee on animal testing. Furthermore, these experiments were approved by the ethical committee of the University of Angers and the regional ethics committee on animal testing (Authorization no. 01315.01 12/2013). Furthermore, animal experiments were carried out in strict accordance with recommendations in the guidelines of the Code for Methods and Welfare Considerations in Behavioral Research with Animals (Directive 2010/63/UE).

Orthotopic model of B16F10 melanoma

C57BL/6 mice have been housed at the university animal facility (Service Commun d'Animalerie Hospitalo-Universitaire—Université d'Angers, France). Syngenic, allograft model of melanoma has been obtained by injecting subcutaneously a suspension of 1.10^6 B16F10 melanoma cells in 100 µL of RPMI into the right flank of mice. Tumour size and tumour volume were monitored until the end of the protocol and have been estimated using the formula: $V = {}^{\pi}/_{6} \times L \times W^2$ (L length and W width). At the end of the protocol, animals have been sacrificed and tumours were removed, frozen in isopentane, and stored at − 80 °C.

Orthotopic model of SK-Mel-28 melanoma

Female nude NMRI mice (Janvier SAS, Le Genest Saint Isle, France) have been housed at the university animal facility. Tumour-bearing mice were prepared by injecting subcutaneously a suspension of 3.10^6 SK-Mel-28 melanoma cells in 100 µL of RPMI into the right flank of mice.

Tumour size and tumour volume were monitored until the end of the protocol and they have been estimated using the formula: $V = {}^{\pi}/_{6} \times L \times W^2$ (L length and W width). At the end of the protocol, animals have been sacrificed and tumours were removed, frozen in isopentane and stored at − 80 °C.

Growth rate measurement and survival

Tumour volume, for each mouse, has been measured at different timepoints. Thereby, the tumour growth rate was calculated according to the formula: $\frac{(\text{tumour volume at given day} - \text{tumour volume of previous measure})}{\text{number of days between measures}}$.

Immunostaining

Mice tumour samples

Frozen tumours were cut into 10 µm sections using Cryotome (CM3050D, Leica, Glattbrugg, Switzerland), and placed onto microscopic slides (Starfrost). Sections were air-dried for 1 h, rehydrated for 15 min in phosphate buffered saline (PBS), fixed by incubation at 4 °C for 10 min in 4% paraformaldehyde/PBS pH 7.4 and permeabilized with 0.02% Triton X-100. Non-specific binding has been blocked

by incubation in PBS containing 4% bovine serum albumin (BSA) and 10% normal goat serum (NGS).

Sections were then incubated with CD31 (BD Biosciences, San Jose, CA, USA, 1/200 diluted) and/or desmin (Dako Denmark A/S, 1/200 diluted) primary antibodies overnight at 4 °C (antibodies have been tested and validated on both mouse and human models). After washing with PBS, samples were treated with a secondary antibody in 5% BSA in PBS for 1 h at room temperature (Table 1). Nuclei were counter stained with 4′,6-diamidino-2-phenylindole (DAPI, Sigma-Aldrich Co.).

Sections were then visualized by confocal microscopy (confocal laser microscope TCS SP8, Leica, Glattbrugg, Switzerland, equipped with 50 mW diode laser) (Clere et al. 2010).

Size of vessel lumens was measured using the Image J Software. Vessel lumens were determined by absence of nuclei surrounded by endothelial cells. Area of vessels was calculated using the formula $= \pi \times R \times r$. Lumen sizes were then classed on a power 10 scale to separate vessels by class size and expressed in function of the percentage of vessels measured by tumours.

Human tumour samples

The material consisted of a retrospective cohort of melanoma samples from 8 patients. All patients provided written informed consent and the study was approved by the local ethic committee and registered under the CNIL#1278197. 5 µm paraffine embedded tissues were done and processed for immunohistochemistry on a Bond III system from Leica. Antibodies used were: anti-CD31 (1/160. clone J770A from Dako) and anti-desmin (1/200. Clone D33 from Dako). Details about patients are summarized in Table 1.

Vessel density and size measurement

The vessel density was assessed according to literature (Hansen et al. 2004). Immunostained tumours were analysed at low magnificent (10×) with a confocal laser microscope (TCS SP8, Leica), or a Leica DMR mounted with Scion CFW-1612C digital color camera (Scion Corporation). Numerous fields of the tumours were pictured, and all vessels were counted using the Image J Software. Micro-vessel density was determined as the number of vessels per mm^2.

Statistical analysis

Results are expressed as boxplot. Each box represents 50% of the distribution (interquartile range: 25th percentile− 75th percentile). Median is marked as a black line in each box. Extending lines from boxes show minimum and maximum values. Outlier data are plot as black circles. Statistical analysis was performed using a Kruskal–Wallis test followed by a Dunn's post-Hoc test with a Hochberg correction using the R software (R Foundation, Austria) with the PMCR package. The level of significance was set at $p < 0.05$. Survival rate has been assessed with the Kaplan–Meier method. The survival probability at any particular time is calculated, over a period time, by the formula: $\frac{(\text{number of alive subjects at the starting point} - \text{number of subjects died})}{\text{number of alive subjects at the starting point}}$.

Results

B16F10 melanoma model grows faster than SK-Mel-28 tumour

Injection of B16F10 melanoma cells in mice induced a detectable tumour with a volume of 100 mm^3 within 7 days after xenograft, whereas SK-Mel-28 cells required 21 days to induce a detectable tumour with the same volume. Furthermore, it should be noted a difference in the duration of the experimental protocols. Thus, the growth of syngenic B16F10-allografted tumour is maximal after 19 days, while tumours induced by SK-Mel-28 cells grew for 49 days. At the end of the protocol, the average volume of B16F10-allografted and SK-Mel-28-xenografted tumours was of

Table 1 Patient clinical characteristics

Patient #	Sex	Age at the time of surgery	Sample type (stage at diagnosis)	Systemic treatment at the time of surgery
1	M	76	Superficial spreading melanoma (stage I)	None
2	M	71	Superficial spreading melanoma (stage I)	None
3	M	78	Superficial spreading melanoma (stage I)	None
4	M	51	Nodular melanoma (stage IV)	None
5	F	88	Nodular melanoma (stage III)	None
6	F	58	Nodular melanoma (stage IV)	None
7	M	42	Nodular melanoma (stage II)	None
8	M	48	Lymph node melanoma metastasis (stage III)	None

Table 2 Characteristics of tumour growth in B16F10-allografted and SK-Mel-28-xenografted mice

	B16F10	SK-Mel-28
Time to reach a volume of 100 mm^3 (days)	7	21
Time to reach the end of the protocol (days)	19	49
Tumour volume at the end of the protocol (mm^3)	4018.47 ± 1179.82	430.00 ± 44.60

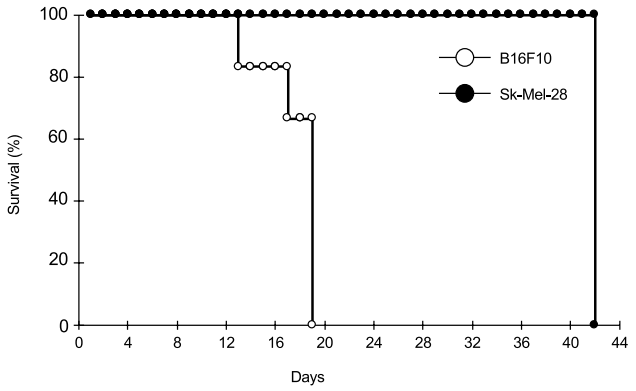

Fig. 1 Kaplan–Meier survival curves for mice with B16F10-allografted ($n=6$) and SK-Mel-28-xenografted ($n=8$) melanoma cells. *P* value ($p=0.00028$) was derived from log-rank calculations

4018.47 ± 1179.82 and 430.00 ± 44.60 mm^3, respectively (Table 2).

B16F10 melanoma model enhances mice mortality in comparison with SK-Mel-28 model

In B16F10-melanoma model, analysis of the survival of tumour-bearing mice revealed a first mortality of 17% and a second mortality of 16% after 13 and 17 days following tumour cell xenograft, respectively. No mortality has been observed in SK-Mel-28-tumour-bearing mice during the protocol. All mice have been sacrificed at day 49 corresponding to the end of the protocol (Fig. 1). Log-rank test analysis showed a significant difference in the survival curve between mice allografted with B16F10 cells and mice xenografted with SK-Mel-28 melanoma cells.

Analysis of vascular density in mice and human melanoma models

Microscopy observations of each tumour revealed an enhancement of CD31 staining in both B16F10-allografted tumour model (Fig. 2a) and human melanoma (Fig. 2c) in comparison with SK-Mel-28-xenografted melanoma model (Fig. 2b). This observation has been confirmed by the analysis of tumour vascular density (expressed by the number of vessels per mm^2) which was significantly enhanced in B16F10-tumour model (20.52 vessels/mm^2) compared to SK-Mel-28 melanoma model (9.05 vessels/mm^2). No difference of vascular density has been found in human melanoma (11.68 vessels/mm^2) in comparison with other mice models (Fig. 2d).

To confirm these first observations, analysis of the vessel number according to the area of their lumen has been realized by microscopy observations on each model. Thus, small vessels (area between 10 and 10^2 μm^2) and vessels with medium area (between 10^2 and 10^3 μm^2) were significantly ($p < 0.05$) enhanced in human tumours in comparison with B16F10 and SK-Mel-28 mice tumours. No difference has been found in the percentage of vessels with lumen size between 10^3 and 10^4 $\mu\mu^2$ whatever the tumour models. Finally, vessels whose area is comprised between 10^4 and 10^5 μm^2 were mainly found in murine tumours with, in particular, a significant increase ($p < 0.05$) in SK-Mel-28 model compared to human tumours (Fig. 3).

Expression of CD31 and desmin in mice and human melanoma models

The distribution pattern of CD31 and desmin was different according to the tumour models. A diffuse and low expression of both CD31 and desmin has been observed in tumours from B16F10 melanoma model (Fig. 4a, b). Furthermore, irregularities in endothelium structure have been found in SK-Mel-28 tumours confirmed by low and discontinuous CD31 expression at the periphery of the vessel lumen. Moreover, a stronger expression of desmin has been reported in these last samples (Fig. 4c, d). A diffuse and low expression of desmin has been found in human tumours (Fig. 4e).

Discussion

Tumour vascular endothelium constitutes a barrier more or less permeable to endogenous mediators or to the molecules used for therapeutic purposes. The present study provides evidence that, depending on melanoma tumour model, many structural and functional differences have been observed in tumour vascular endothelium. Thus, while tumour growth is faster in B16F10 than in SK-Mel-28 melanoma model, vascular density in B16F10 tumour model is significantly enhanced compared to SK-Mel-28 and human tumours. Furthermore, while vessels from human melanoma present lumen size between

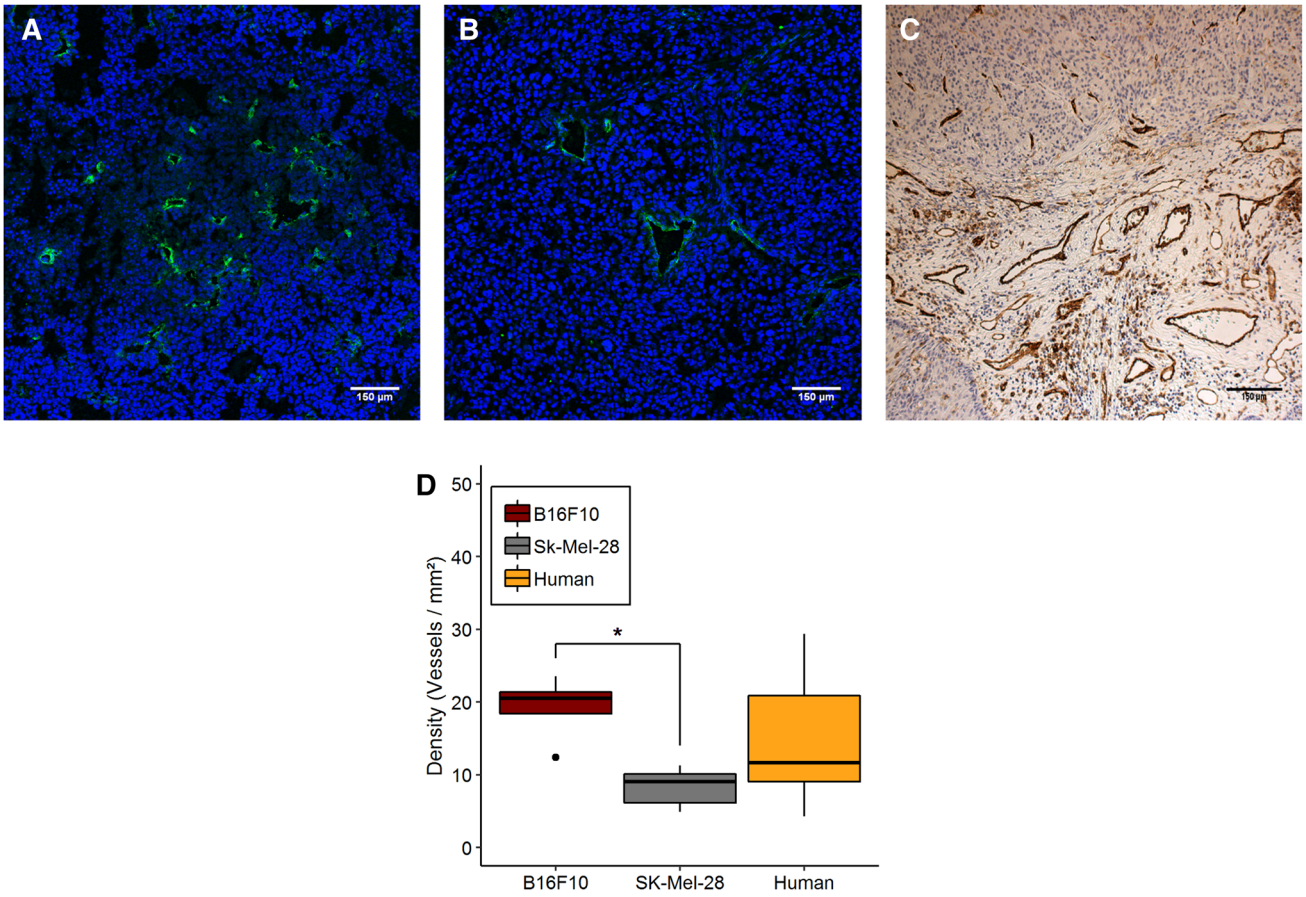

Fig. 2 Confocal microscopy of B16F10 (**a**), SK-Mel-28 (**b**). Endothelial cells were labelled with CD31 antibodies (green fluorescence), while nuclei were labelled with DAPI (Blue). Scale bar: 150 µm. **c** Analysis of human melanoma tumour. Endothelial cells were labelled with CD31 antibodies (brown staining) Scale bar: 150 µm. **d** Microvascular density according to the study model. Results were presented in a boxplot, where bottom and top line of each box correspond to the 25th and 75th percentiles, respectively $*p \leq 0.05$. B16F10 $n=4$, SK-Mel-28 $n=8$, human melanoma $n=8$

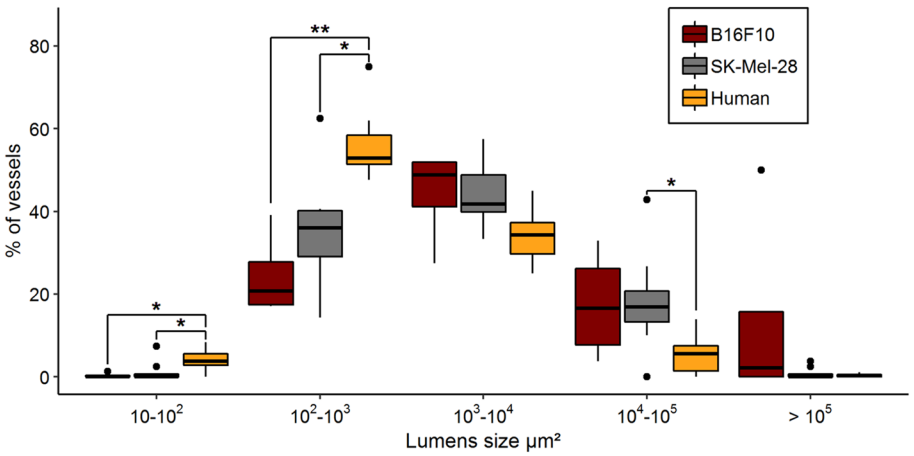

Fig. 3 Area of vessels according to the percentage of vessels measured in B16F10, SK-Mel-28 and human melanoma. The significance value was calculated using a Kruskal–Wallis test followed by a Dunn's post-Hoc test with a Hochberg correction $*p \leq 0.05$; $**p \leq 0.01$. B16F10 $n=4$, SK-Mel-28 $n=8$, human melanoma $n=8$

10 and 10^3 µm^2, B16F10 and SK-Mel-28 mice tumours develop significantly larger vessels with a lumen size comprised between 10^4 and 10^5 µm^2. These last differences in vascularization were followed accompanied by structural abnormalities confirmed by a defect in CD31 and desmin expressions in B16F10 model, in comparison with

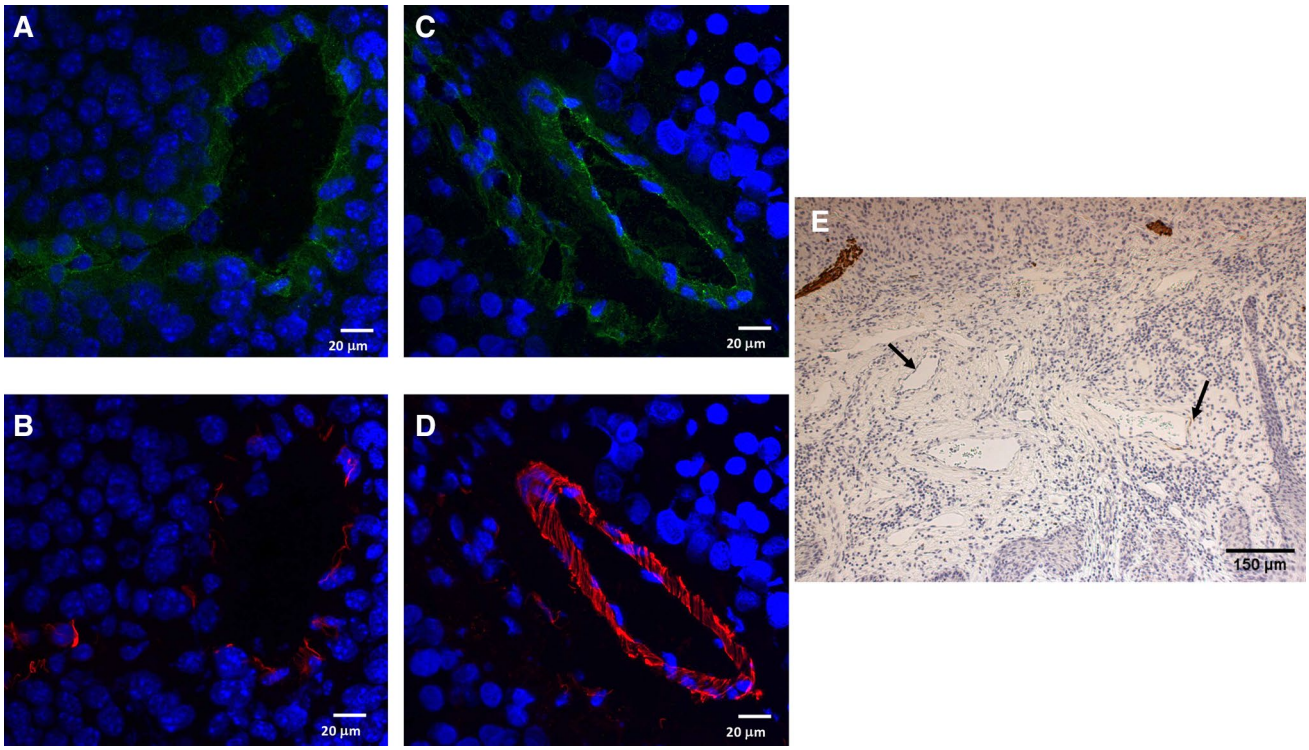

Fig. 4 Confocal microscopy of **a, b** B16F10 and **c, d** SK-Mel-28 tumour sections at a magnificence of 60X. **e** Microscopy of human tumour sections at a magnificence of 10X. **a–c** Endothelial cells were labelled with CD31 antibodies (green), **b–d** pericytes were labelled with desmin (red). Nuclei were labelled with DAPI (blue). Scale bar: 20 µm. **e** Pericytes, showed by the arrow, were labelled with desmin and were revealed through peroxidase. Scale bar: 150 µm

SK-Mel-28 tumour model. Analysis of human samples showed a significant expression of CD31, while a diffuse and low expression of desmin has been found.

In the present study, two protocols have been used to induce mice melanoma. A first model was obtained following the xenograft of 3.10^6 SK-Mel-28 cells in *nude* mice for 42 days. In this tumour model, a slow tumour growth reaching a volume of 100 mm^3 in 21 days has been observed. These data are different from those obtained with a second B16F10 tumour model. In this case, only 10^6 B16F10 melanoma cells are sufficient to induce tumours, whose volume reaches 100 mm^3 after 7 days. Furthermore, as shown in Fig. 1, mortality is significantly enhanced in mice allografted with B16F10 melanoma, in comparison with mice inoculated with SK-Mel-28. These results can be explained by differences in selected cell models. First, B16F10 cells have a significantly lower doubling time than the SK-Mel-28 cells: 17.2 h (Danciu et al. 2013) for B16F10 vs 72 h for SK-Mel-28 cells (Wahl et al. 2002). Moreover, the analysis of VEGF expression by these both cell models showed that melanoma model induced by SK-Mel-28 cells expressed much less VEGF (Kim et al. 2009) than by B16F10 cells (Danciu et al. 2015). Thus, all of these data suggest that B16F10 cells are more aggressive than SK-Mel-28 cells, explaining the differences in tumour growth observed from these melanoma models.

As described by a multivariate analysis, tumour vascularity, even more than the tumour thickness, is the most important determinant of its overall growth (Kashani-Sabet et al. 2002). Thus, as for all solid tumours, melanoma growth needs a high angiogenic activity, an important step in melanoma metastasis (Elder et al. 1996; Tuthill and Reed 2007). Angiogenesis is a dynamic process that involves different stages and, in particular, the activation of endothelial cells to form new vessels. These abnormal tumour vessels are characterized by a mal-shaped, irregular, disorganized, and tortuous architecture with a highly dysfunctional and leaky endothelial cell layer (De Bock et al. 2009, 2011; Jain 2005). In the present study, confocal microscopy revealed a low expression of CD31 expression in each tumour model. This finding suggests the existence of structural abnormalities in tumour endothelium from mice models as previously described in B16F10 by Duncan et al. (2013).

Immunolabeling data revealed very few (if any) expression of pericytes at the surface of tumour vessels from B16F10. While a greater expression of pericytes has been found at the surface of vessels from SK-Mel-28, only half of the identified vessels significantly expressed desmin, the

other half did not express it. These findings suggest that for fast-growing tumour models (such as B16F10), vascular patterning is incomplete, whereas for slow-growth models (as SK-Mel-28), the vessels appear to be better structured and organized and may be more impermeable than vessels from B16F10.

A limitation in the experimental design could have been the inequitable use of C57BL/6 mice for B16F10 tumours vs the use of nude mice for SK-Mel-28 tumours. Given the importance of the overall tumour micro-environment for controlling various steps of tumorigenesis (Palazon et al. 2017), it would have been difficult to make comparisons on the two different tumours using two different hosts. For instance, while the immune compromised nude mice still possess innate immunity, they are deficient in components of acquired immunity. Since regulatory T cells and gamma-delta T cells have both been implicated in promoting tumour vascularization (Fleming et al. 2017), the nude hosts will be deficient in this aspect of tumours blood vessel development. For these reasons, and because the vasculature is derived from the host rather than the tumour, we evaluated vascular density and tumour vessels' structure in human melanoma models collected from immunocompetent patients. Thus, we have reported a vascular density identical to what found in SK-Mel-28 model but which proves not to be significantly different from what observed for B16F10 model. These data suggest that immune defect observed in nude mice cells does not influence microvascular density, as it may have been reported for some human primary oral melanoma by Simonetti et al. (2013). Microscopic analyses confirm an anarchic organization of human tumour vessels, characterized by a low expression of CD31 and a very weak expression of desmin. The analysis of the vascularization, according to the lumen size confirms the presence of capillaries, with a small caliber (10–10^3 μm^2) in these samples. These findings have been reported in primary cutaneous melanomas of the scalp and neck, in which it has been found a correlation between melanoma growth and both vessel invasion and higher density (Pasquali et al. 2015).

The enhanced permeability and retention (EPR) effect is defined as a process of extravasation of large molecules from leaky tumour vasculature, leading to accumulation in tumour tissue (Matsumura and Maeda 1986). Newly formed blood vessels typically occur in higher density in tumour tissue (Vakoc et al. 2009), they often lack a smooth muscle layer and pericytes (Nagy et al. 2009), they have large lumen and wider fenestrations (Hashizume et al. 2000), and they typically contain malfunctioning endothelial cells (Dudley 2012). In addition, vascular perfusion tends to be impaired, at least to some extent, and blood flow is sluggish (Hori et al. 1991, 2000). Several of these features are described in our study mainly in the B16F10 model compared to the SK-Mel-28 or human model. Based on these data and results, we could hypothesize that B16F10 melanoma model presents a more pronounced EPR effect than SK-Mel-28 or human model.

Several authors have described the EPR effect as essential for improving tumour-targeting of therapeutics (Stylianopoulos and Jain 2015; Taniguchi et al. 2003). For instance, it has been reported for Doxil®, the first FDA-approved nanodrug, that it is passively targeted to tumours through the potentiation of EPR effect (Barenholz 2012). Thereby, the high permeability of tumour blood vessels would induce an important fluid loss from the vessel to the interstitial space, which could reduce tumour perfusion and further enhance the delivery of nanoparticles (Danhier et al. 2015; Stylianopoulos and Jain 2013).

However, these encouraging data should not mask the limitations of the therapeutic distribution through EPR effect. Thus, the theories described above are not sufficient (Hollis et al. 2013), because authors hypothesized that the EPR effect would restrict the delivery of various drugs, mainly in human tumours (Jain 2001; Jain and Stylianopoulos 2010). While using the EPR effect as a rationale for nanoparticles, it is often overlooked that not all tumour vessels are leaky, which causes a heterogeneous distribution of pore sizes and thus heterogeneous extravasation and delivery. Moreover, the permeability in tumour models depends on the transplantation site and varies with time and in response to treatment. Because tumours are usually faster-growing in animal models, it is to be expected that they will have a higher degree of vascularization and a less developed vascular environment, leading to a high EPR effect (Bolkestein et al. 2016). Therefore, it has been suggested by various authors (Lammers et al. 2012) and recently by Danhier (2016) that the EPR effect would be different in rodents than in humans. On one hand, human tumours develop usually from a cell or small group of cells, and it can take years before these cells develop a set of mutations required to escape from the immune system and form tumour (Kim et al. 2007). This period lets tumour cells interact with surrounding cells and develop a highly heterogeneous and complex micro-environment (Egeblad et al. 2010). Furthermore, tumours are composed of heterogeneous cells containing subpopulations with various mutations, giving a diversity of mutated cells and resistance to treatment (Choi et al. 2011). On the other hand, unlike human tumours, animal models are usually obtained by implantation of a large number of tumour cells, growing generally in few weeks. Due to this fast growth, tumour cells can escape to the immune system and are not willing to develop the genetic diversity observed in natural human tumours. It seems that these differences have implications on the structure of tumour vessels, and therefore, they impact the leakage of macromolecules or nanomedicines.

Our present study seems to confirm this hypothesis and suggests that human melanoma develop anarchic capillaries to bring oxygen and nutrients to the tumour, while mice models have anarchic vessels with high lumen size probably more permeable to macromolecules or drugs. The highly variable nature of tumour models, which is a result of various genetic mutations (and whose development conditions are different), leads to an enormously high heterogeneity in the vascularization of tumours, in the EPR effect on these tumours, and, therefore, in the anti-tumour responses of therapeutic agents. Our study confirms that, when aiming to develop nanomedicines for clinical use, the heterogeneity of vascularization and the EPR effect has to be taken into account and both combining studies on various models and new strategies have to be developed to overcome this obstacle.

Acknowledgements The authors thank the "service commun imagerie et analyse microscopique" and particularly Dr. Mabilleau and Dr. Perrot for their expertise. We are also grateful to Ms. Dumez and Ms. Viau for their technical support.

Funding The authors thank the "comité départemental du Maine et Loire de la Ligue contre le Cancer" for its financial support for the realization of this project. Furthermore, the authors would like to thank the "Région Pays de la Loire" and the "Erasmus Mundus" program for the financing of the phD program of VP.

Compliance with ethical standards

Conflict of interest The authors declare that they have no conflict of interest.

Ethical approval All applicable international, national, and/or institutional guidelines for the care and use of animals were followed.

Informed consent Informed consent was obtained from all individual participants included in the study.

References

Armulik A, Genove G, Betsholtz C (2011) Pericytes: developmental, physiological, and pathological perspectives, problems, and promises. Dev Cell 21:193–215. https://doi.org/10.1016/j.devcel.2011.07.001

Baluk P, Hashizume H, McDonald DM (2005) Cellular abnormalities of blood vessels as targets in cancer. Curr Opin Genet Dev 15:102–111. https://doi.org/10.1016/j.gde.2004.12.005

Barenholz Y (2012) Doxil®--the first FDA-approved nano-drug: lessons learned. J Control Release 160:117–134. https://doi.org/10.1016/j.jconrel.2012.03.020

Bolkestein M, de Blois E, Koelewijn SJ, Eggermont AM, Grosveld F, de Jong M, Koning GA (2016) Investigation of factors determining the enhanced permeability and retention effect in subcutaneous Xenografts. J Nucl Med 57:601–607. https://doi.org/10.2967/jnumed.115.166173

Carmeliet P, Jain RK (2000) Angiogenesis in cancer and other diseases Nature 407:249–257. https://doi.org/10.1038/35025220

Chan RC, Babbs CF, Vetter RJ, Lamar CH (1984) Abnormal response of tumor vasculature to vasoactive drugs. J Natl Cancer Inst 72:145–150. https://doi.org/10.1093/jnci/72.1.145

Choi YP, Shim HS, Gao MQ, Kang S, Cho NH (2011) Molecular portraits of intratumoral heterogeneity in human ovarian cancer. Cancer Lett 307:62–71. https://doi.org/10.1016/j.canlet.2011.03.018

Clere N et al (2010) Deficiency or blockade of angiotensin II type 2 receptor delays tumorigenesis by inhibiting malignant cell proliferation and angiogenesis. Int J Cancer 127:2279–2291. https://doi.org/10.1002/ijc.25234

Danciu C et al (2013) A characterization of four B16 murine melanoma cell sublines molecular fingerprint and proliferation behavior. Cancer Cell Int 13:75. https://doi.org/10.1186/1475-2867-13-75

Danciu C et al (2015) Behaviour of four different B16 murine melanoma cell sublines: C57BL/6J skin Int. J Exp Pathol 96:73–80. https://doi.org/10.1111/iep.12114

Danhier F (2016) To exploit the tumor microenvironment: since the EPR effect fails in the clinic, what is the future of nanomedicine? J Control Release 244:108–121. https://doi.org/10.1016/j.jconrel.2016.11.015

Danhier F et al (2015) Paclitaxel-loaded micelles enhance transvascular permeability and retention of nanomedicines in tumors. Int J Pharm 479:399–407. https://doi.org/10.1016/j.ijpharm.2015.01.009

Danquah MK, Zhang XA, Mahato RI (2011) Extravasation of polymeric nanomedicines across tumor vasculature Adv Drug Deliv Rev 63:623–639. https://doi.org/10.1016/j.addr.2010.11.005

De Bock K, De Smet F, Leite De Oliveira R, Anthonis K, Carmeliet P (2009) Endothelial oxygen sensors regulate tumor vessel abnormalization by instructing phalanx endothelial cells. J Mol Med (Berl) 87:561–569. https://doi.org/10.1007/s00109-009-0482-z

De Bock K, Cauwenberghs S, Carmeliet P (2011) Vessel abnormalization: another hallmark of cancer? Molecular mechanisms and therapeutic implications. Curr Opin Genet Dev 21:73–79. https://doi.org/10.1016/j.gde.2010.10.008

Dudley AC (2012) Tumor endothelial cells Cold Spring. Harb Perspect Med 2:a006536. https://doi.org/10.1101/cshperspect.a006536

Duncan R, Sat-Klopsch YN, Burger AM, Bibby MC, Fiebig HH, Sausville EA (2013) Validation of tumour models for use in anticancer nanomedicine evaluation: the EPR effect and cathepsin B-mediated drug release rate. Cancer Chemother Pharmacol 72:417–427. https://doi.org/10.1007/s00280-013-2209-7

Egeblad M, Nakasone ES, Werb Z (2010) Tumors as organs: complex tissues that interface with the entire organism. Dev Cell 18:884–901. https://doi.org/10.1016/j.devcel.2010.05.012

Elder DE, Van Belle P, Elenitsas R, Halpern A, Guerry D (1996) Neoplastic progression and prognosis in melanoma Semin Cutan Med Surg 15:336–348. https://doi.org/10.1016/s1085-5629(96)80047-2

Fleming C, Morrissey S, Cai Y, Yan J (2017) γδ T cells: unexpected regulators of cancer development and progression Trends Cancer 3:561–570. https://doi.org/10.1016/j.trecan.2017.06.003

Folkman J (2002) Role of angiogenesis in tumor growth and metastasis Semin Oncol 29:15–8 https://doi.org/10.1053/sonc.2002.37263

Hanahan D, Weinberg RA (2000) The hallmarks of cancer Cell 100:57–70. https://doi.org/10.1016/S0092-8674(00)81683-9

Hanahan D, Weinberg RA (2011) Hallmarks of cancer: the next generation Cell 144:646–674. https://doi.org/10.1016/j.cell.2011.02.013

Hansen S, Sørensen FB, Vach W, Grabau DA, Bak M, Rose C (2004) Microvessel density compared with the Chalkley count in a prognostic study of angiogenesis in breast cancer patients Histopathology 44:428–436. https://doi.org/10.1111/j.1365-2559.2004.01848.x

Hashizume H et al (2000) Openings between defective endothelial cells explain tumor vessel leakiness. Am J Pathol 156:1363–1380. https://doi.org/10.1016/s0002-9440(10)65006-7

Hollis CP, Weiss HL, Leggas M, Evers BM, Gemeinhart RA, Li T (2013) Biodistribution and bioimaging studies of hybrid paclitaxel nanocrystals: lessons learned of the EPR effect and image-guided drug delivery. J Control Release 172:12–21. https://doi.org/10.1016/j.jconrel.2013.06.039

Hori K, Suzuki M, Tanda S, Saito S, Shinozaki M, Zhang QH (1991) Fluctuations in tumor blood flow under normotension and the effect of angiotensin II-induced hypertension Jpn. J Cancer Res 82:1309–1316. https://doi.org/10.1111/j.1349-7006.1991.tb01797.x

Hori K, Saito S, Takahashi H, Sato H, Maeda H, Sato Y (2000) Tumor-selective blood flow decrease induced by an angiotensin converting enzyme inhibitor, temocapril hydrochloride Jpn J Cancer Res 91:261–269. https://doi.org/10.1111/j.1349-7006.2000.tb00940.x

Jain RK (2001) Delivery of molecular medicine to solid tumors: lessons from in vivo imaging of gene expression and function. J Control Release 74:7–25. https://doi.org/10.1016/s0168-3659(01)00306-6

Jain RK (2005) Normalization of tumor vasculature: an emerging concept in antiangiogenic therapy Science 307:58–62. https://doi.org/10.1126/science.1104819

Jain RK, Baxter LT (1988) Mechanisms of heterogeneous distribution of monoclonal antibodies and other macromolecules in tumors: significance of elevated interstitial pressure. Cancer Res 48:7022–7032

Jain RK, Stylianopoulos T (2010) Delivering nanomedicine to solid tumors. Nat Rev Clin Oncol 7:653–664. https://doi.org/10.1038/nrclinonc.2010.139

Kashani-Sabet M, Sagebiel RW, Ferreira CM, Nosrati M, Miller JR (2002) Tumor vascularity in the prognostic assessment of primary cutaneous melanoma. J Clin Oncol 20:1826–1831. https://doi.org/10.1200/JCO.2002.07.082

Kim R, Emi M, Tanabe K (2007) Cancer immunoediting from immune surveillance to immune escape Immunology 121:1–14. https://doi.org/10.1111/j.1365-2567.2007.02587.x

Kim JY et al (2009) The expression of VEGF receptor genes is concurrently influenced by epigenetic gene silencing of the genes and VEGF activation Epigenetics 4:313–321

Lammers T, Kiessling F, Hennink WE, Storm G (2012) Drug targeting to tumors: principles, pitfalls and (pre-) clinical progress. J Control Release 161:175–187. https://doi.org/10.1016/j.jconrel.2011.09.063

Matsumura Y, Maeda H (1986) A new concept for macromolecular therapeutics in cancer chemotherapy: mechanism of tumoritropic accumulation of proteins and the antitumor agent smancs. Cancer Res 46:6387–6392

McDonald DM, Thurston G, Baluk P (1999) Endothelial gaps as sites for plasma leakage in inflammation Microcirculation 6:7–22. https://doi.org/10.1080/713773924

Nagy JA, Chang SH, Dvorak AM, Dvorak HF (2009) Why are tumour blood vessels abnormal and why is it important to know? Br J Cancer 100:865–869. https://doi.org/10.1038/sj.bjc.6604929

Palazon A et al (2017) An HIF-1α/VEGF-A axis in cytotoxic T cells regulates tumor progression Cancer Cell 32:669–683.e665. https://doi.org/10.1016/j.ccell.2017.10.003

Pasquali S et al (2015) Lymphatic and blood vasculature in primary cutaneous melanomas of the scalp and neck. Head Neck 37:1596–1602. https://doi.org/10.1002/hed.23801

Simonetti O et al (2013) Microvessel density and VEGF, HIF-1α expression in primary oral melanoma: correlation with prognosis. Oral Dis 19:620–627. https://doi.org/10.1111/odi.12048

Stirland DL, Nichols JW, Miura S, Bae YH (2013) Mind the gap: a survey of how cancer drug carriers are susceptible to the gap between research and practice. J Control Release 172:1045–1064. https://doi.org/10.1016/j.jconrel.2013.09.026

Stylianopoulos T, Jain RK (2013) Combining two strategies to improve perfusion and drug delivery in solid tumors. Proc Natl Acad Sci U S A 110:18632–18637. https://doi.org/10.1073/pnas.1318415110

Stylianopoulos T, Jain RK (2015) Design considerations for nanotherapeutics in oncology Nanomedicine 11:1893–1907. https://doi.org/10.1016/j.nano.2015.07.015

Taniguchi M, Seino K, Nakayama T (2003) The NKT cell system: bridging innate and acquired immunity. Nat Immunol 4:1164–1165. https://doi.org/10.1038/ni1203-1164

Tuthill RJ, Reed RJ (2007) Failure of senescence in the dysplasia-melanoma sequence: demonstration using a tissue microarray and a revised paradigm for melanoma. Semin Oncol 34:467–475. https://doi.org/10.1053/j.seminoncol.2007.09.014

Vakoc BJ et al (2009) Three-dimensional microscopy of the tumor microenvironment in vivo using optical frequency domain imaging. Nat Med 15:1219–1223. https://doi.org/10.1038/nm.1971

Wahl ML et al (2002) Regulation of intracellular pH in human melanoma: potential therapeutic implications. Mol Cancer Ther 1:617–628